Lithium dendrite and solid electrolyte interphase investigation using OsO$_4$

Martin Zier [a,b], Frieder Scheiba [c,d,*], Steffen Oswald [a], Jürgen Thomas [a], Dietrich Goers [e], Torsten Scherer [f], Markus Klose [a], Helmut Ehrenberg [c,d], Jürgen Eckert [a,b]

[a] IFW Dresden, Institute for Complex Materials, Helmholtzstraße 20, D-01069 Dresden, Germany
[b] Dresden University of Technology, Institute of Materials Science, Helmholtzstraße 7, D-01069 Dresden, Germany
[c] Karlsruhe Institute of Technology (KIT), Institute for Applied Materials (IAM), Hermann-von-Helmholtz-Platz 1, D-76344 Eggenstein-Leopoldshafen, Germany
[d] Helmholtz-Institute Ulm for Electrochemical Energy Storage (HIU), P.O. Box 3640, D-76021 Karlsruhe, Germany
[e] Li-Tec Battery GmbH, Am Wiesengrund 7, D-01917 Kamenz, Germany
[f] Karlsruhe Institute of Technology (KIT), Institute of Nanotechnology (INT), Hermann-von-Helmholtz-Platz 1, D-76344 Eggenstein-Leopoldshafen, Germany

HIGHLIGHTS

- Osmium tetroxide (OsO$_4$) staining greatly improves material contrast in LIB electrodes.
- Detection and study of distribution of lithium dendrites on graphitic anodes possible.
- Coordinated reaction of OsO$_4$ with components of the SEI is shown.
- Electrochemically removed lithium dendrites can be located by their stained SEI shells.
- Applicable for cross sectional study of Li dendrite distribution and SEI layer evolution.

GRAPHICAL ABSTRACT
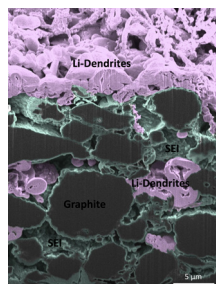
ARTICLE INFO

ABSTRACT

Osmium tetroxide (OsO$_4$) staining, commonly used to enhance scattering contrast in electron microscopy of biologic tissue and polymer blends, has been adopted for studies of graphite anodes in lithium-ion batteries. OsO$_4$ shows a coordinated reaction with components of the solid electrolyte interphase (SEI) and lithium dendrites, thereby increasing material contrast for scanning electron microscopy investigations. Utilizing the high affinity of lithium metal to react with osmium tetroxide it was possible to localize even small lithium deposits on graphite electrodes. In spite of their reaction with the OsO$_4$ fume, the lithium dendrite morphology remains almost untouched by the staining procedure, offering information on the dendrite growth process. Correlating the quantity of osmium detected with the amount of residual ("dead") lithium of a discharged electrode, it was possible to obtain a practical measure for lithium plating and stripping efficiencies. EDX mappings allowed for a localization of electrochemically stripped lithium dendrites by their residual stained SEI shells. Cross sections, prepared by focused ion beam (FIB) of cycled graphite electrodes treated with OsO$_4$, revealed important information about deposition and distribution of metallic lithium and the electrolyte reduction layer across the electrode.

© 2014 Elsevier B.V. All rights reserved.

* Corresponding author. Karlsruhe Institute of Technology (KIT), Institute for Applied Materials (IAM), Hermann-von-Helmholtz-Platz 1, D-76344 Eggenstein-Leopoldshafen, Germany. Tel.: +49 721 608 28520.
E-mail address: frieder.scheiba@kit.edu (F. Scheiba).

1. Introduction

Most of today's Lithium-ion batteries use graphitic carbons as the negative electrode material because of its advantageous properties such as safety, price and cycling stability. The comparably low gravimetric capacity, however, renders it unsuitable for future's battery demands, re-fueling the interest in lithium metal that offers highest energy-density and specific capacity. Yet, both electrode materials face one issue alike: they are prone to surface-mediated lithium deposition of non-uniform characteristics. Such lithium plating is responsible for a fast decay of battery performance and poses high safety risks. Huge efforts were made in order to tackle the susceptibility to dendritic growth of lithium. The appearance of lithium deposits is closely linked to the surface chemistry of the electrode material [1], the electrolyte composition [2–6], salt concentration [7], surface morphology [8–10] as well as the degree of graphitization [11]. Co-deposition of sodium [12–14] and the addition of small concentrations of Cs^+ have proven beneficial to reduce dendritic growth [15]. Most of the visualization methods applied (optical cells [2,4,16], AFM [17], NMR [18], electron microscopy [8,15,19–21]) are dedicated to study lithium deposition morphology after or during electrochemical testing [17,18,20,21]. Only little work on the quantification of lithium deposition has been reported so far [22]. The poor coulombic efficiencies [1,3,11,14,19], that are a main attribute of lithium plating due to electrolyte reduction, have not been studied quantitatively using scanning electron microscopy. Providing accurate data is particularly difficult when investigating lithium deposition on graphite electrodes. The low material contrast provided, allows only small sections (high magnifications) of the electrodes to be investigated properly, thus impeding the effective analysis of overall deposition distribution. However, in order to estimate the effects of lithium deposition on electrode performance it is inevitable to gain quantitative results beyond the actual electrochemical data.

Most of the improvements achieved on controlling lithium deposition are at least indirectly attributed to a homogenization of current distribution [8,9,23,24]. It was shown that the local current can deviate strongly from the experimentally obtained mean value [25], making it possible for lithium deposition to occur at potentials positive to the thermodynamic reduction potential [16]. Thus, lithium deposition is directly correlated to locally deteriorated current density distribution which in turn is strongly linked to the solid electrolyte interphase (SEI) [26] as a determining factor on surface homogeneity, battery cycle life and overall cell performance [27,28]. Several techniques were applied in order to analyze the complex composition and multilayer structure of the SEI [29–33], yet many features of it remain obscure [34]. The continuous improvement of technologies visualizing the microstructure of materials, however, allowed first electron microscopy studies of changes in SEI thickness with cycling [30] and observation of morphology dependence on formation conditions [35,36] and electrolyte composition [37].

As is for lithium deposited on graphite, studying the electrolyte reduction layer is hardly possible when using electron microscopy techniques due to the low scattering contrast of its components and its instability in the electron beam [30,37,38]. Biology and polymer science have overcome comparable difficulties where samples like (human) body cells and polymer blends with very low material contrast are subject to studies using (transmission) electron microscopy. A common technique in these fields which was first applied by Kato in 1965 [39] to polymers, is the selective staining of double-bonds by osmium tetroxide [40–45]. While the well-known reactivity of OsO_4 with butadiene based rubbers has previously been used in lithium-ion battery research to investigate the distribution of CMC-SBR binders within the electrode, we herein report a new application of the OsO_4 staining technique to study lithium deposition and the SEI layer on graphite electrodes. The staining resulted in a dramatic improvement of material contrast when using electron microscopy along with a stabilization of the samples against air exposure as well as beam induced damage. In a first principles study we were able to illustrate the application for a much improved detection and quantification of lithium dendrites and dead-lithium in graphite electrodes not reported using electron microscopy so far. Additionally, a coordinated reaction of the SEI with osmium tetroxide is shown, allowing for a better study of its morphological changes over life time. This method is therefore able to contribute to both, understanding of lithium deposition and SEI evolution.

2. Materials and methods

2.1. Electrochemical testing

The graphite electrodes used for electrochemical testing and subsequent OsO_4-staining were prepared from a slurry of graphite (MCMB MTI Corp.) with 5% PVdF (Solvay) binder and 3% carbon black (Timcal) in a weight ratio of 92:5:3 using the 'doctor blade' technique. The obtained electrode sheets were allowed to dry overnight at 80 °C. Electrodes of 12 mm diameter were punched from the electrode foil and stored in a vacuum oven for at least 24 h at 100 °C to remove residual moisture. T-shaped three-electrode Swagelok cells were used to allow precise control of the working electrode potential using metallic lithium foil (high-purity, Merck) as counter and as reference electrode in a 1 M LP30 electrolyte (Merck). The electrodes were electrically isolated from each other by two sheets of Whatmann® glass fiber separator of 13 mm in diameter to avoid short circuiting. Cell assembly and disassembly was done in an argon filled glove box (MBraun). The electrochemical measurements were carried out using a VMP3 multichannel potentiostat (Bio-Logic). Uniform SEI formation was achieved by cycling the cells three times between 1.5 V and 0.005 V against Li^+/Li at a current of C/10 based on the active mass of the electrode. Further cycling was done at a C/2 current in the same potential range for 50 times. Cells for slice and view investigation were subject to subsequent forced lithium deposition by overcharging the electrodes to 150% state of charge with a C/10 current. Lithium deposition experiments were performed in potential step mode (PITT) controlling the amount of charge transferred in the same cell setup with either graphite or the sole copper current collector as a working electrode. Prior to disassembly, the electrodes were fully discharged in a constant potential step at 1.5 V until a cut-off current of C/50 was reached. For further investigations, all samples were washed in DMC and dried in vacuum shortly in order to remove residual conductive salt.

2.2. Osmium tetroxide staining

In general, the exposure of samples to osmium (VIII) oxide vapor must be done in strict accordance with the recommended safety guidelines as it is highly toxic, corrosive and volatile. Crystalline osmium tetroxide of 99.8% purity was obtained from Merck KGaA. A special exposure device was constructed in-house to allow both, safe storage of the OsO_4, and sample staining in the osmium tetroxide fume. All samples were put into the exposure chamber from within the argon-filled box. Firmly tightened, the exposure device was transferred to a fume hood where the valve connecting the OsO_4-crystal with the exposure chamber was opened. The average exposure time was chosen between 12 h and 18 h [46] to allow for a complete reaction of the samples with the oxidant. Once staining had been finished, the purge valves were opened and the exposure

chamber was flushed with argon for two hours to remove the unreacted OsO_4 from the samples. The waste gas was passed into a 1 M NaOH solution.

2.3. Spectroscopic and structural investigation

A Mo-Kα x-ray source ($\lambda = 0.70932$ nm) was used on an STOE STADI P diffractometer in transmission mode to analyze the crystal structure of the samples. Angles from 2 theta = $3°-60°$ were investigated whilst permanent rotation of the sample to improve crystallite orientation statistics. A pristine graphite electrode and pure metallic lithium foil were exposed to OsO_4 and probed for their osmium content using photo electron spectroscopy (XPS). To avoid any contact of the samples with air and moisture a transfer chamber (Physical Electronics) was used for the sample transport from the argon-filled glove box to the XPS spectrometer. Oxidation states were analyzed on a PHI 5600 CI (Physical Electronics) spectrometer with an analysis area of 800 μm diameter determined by the hemispherical analyzer that operates at a typical pass energy of 29 eV. Al Kα excitation (350 W) was used and a low energy electron charge neutralizer was additionally applied. Sputter cleaning was done using Ar^+-ions at 3.5 keV at a calculated erosion rate of around 5 nm min^{-1} calibrated to SiO_2. Since the Os 4d and Os 4f contributions overlap with the C 1s and Li 1s binding energies all spectra were corrected based on the Os 4p3/2 main peak. Sample morphology was analyzed using an SEM LEO (Zeiss) with a Gemini I Column equipped an energy dispersive x-ray spectrometer (EDX) for chemical analysis. Elemental mappings (600 × 600 pixels) were taken at 20 kV excitation and a 120 μm aperture within 5 min acquisition time.

2.4. Preparation of TEM samples

Active material was removed from the cycled graphite electrodes by scraping, immersed in a glass vial filled with DMC and dispersed by stirring. A TEM copper grid covered with a lacey carbon film was dipped into the suspension, leaving behind finely distributed graphite particles on the film. The loaded TEM grid was subsequently exposed to OsO_4 vapor. High resolution imaging was conducted using a Tecnai F30 at an accelerating voltage of 300 kV. Electron energy loss spectroscopy (EELS) and EDX were applied to investigate the chemical composition of the samples.

2.5. Preparation of and FIB slice and view samples

Cross sections of an overcharged graphite electrode were prepared by focused ion beam (FIB) on an XBeam 1540-EsB (Zeiss) dual beam scanning electron microscope. A 30 μm × 30 μm platinum pad with 4 μm thickness was deposited on top of the sample. A 30 μm deep trench was milled normal to the sample surface using Ga^+-ion sputtering to unbury the electrode and to allow the slicing debris to collate around the sample. The FEI slice and view software was setup to cut 250 slices with a thickness of 105 nm each taking an SEM picture after each milling step (see Video in the Supporting information).

Supplementary video related to this article can be found at http://dx.doi.org/10.1016/j.jpowsour.2014.04.134

3. Results and discussion

3.1. Morphological studies

HR-TEM investigations of stained and unstained graphite particles were performed to assess the reactions of osmic acid with the solid electrolyte interphase. Atomic layers of the untreated graphite active material can be clearly seen from Fig. 1a. Distorted graphite layers are visible on the particle's surface interspersed by dark crystallites of different atomic layer distance in the case of stained active material (Fig. 1b). Changing the focus plane reveals the graphitic layers similar to the pristine sample (Fig. 1c). Assuming that the graphite particle is surrounded by an SEI, the graphitic features are more or less superimposed by the characteristics of the stained SEI depending on the position of focus. The most prominent feature in the HR-TEM micrographs is the finely dispersed dark crystallites of sizes smaller than 2 nm. These are spread across the entire stained sample and are assigned to the SEI having selectively reacted with OsO_4 to form osmium rich crystals. Lower magnifications were used for the TEM micrograph of Fig. 1d using another, aged graphite electrode sample. A considerable change in thickness of the sample from left to right exposes a heterophase area of approximately 60 nm extent at the edge of the graphite particle. Lucid phases are clearly separated from darker, stained phases. They are of different angular shape perfectly reproducing the heterophase composition of the SEI proposed by Peled [47]. It becomes evident that different SEI components are being stained differently. The transparent phases could be attributed to components like LiF or Li_2O showing least or no reaction with OsO_4. Darker phases, showing dark spots as observed in Fig. 1a and b also, should be attributed to alkyl carbonates and other organic electrolyte reduction products. According to the preferred osmium tetroxide reaction one would expect the outer, polymeric part of the SEI to react more readily than the inner, inorganic part. Yet, the micrographs do not reflect this correlation directly, most likely because the sample does not represent a perfect cut through the SEI. In order to identify gradients in the osmium distribution between the outer and inner parts of the SEI, cross sections of the SEI layer would be necessary. This could only be achieved by dedicated FIB or ion polishing sample preparation which is beyond the scope of this first principle manuscript.

High-Angle Annular Dark-Field imaging (HAADF) of the aged sample shows very bright regions that can be attributed to lithium deposits having readily reacted with osmium tetroxide. The electrochemical cycling protocol of the electrode allows for lithium deposition to occur on the graphite particles. As metallic lithium is an excellent electron donor, osmium tetroxide preferably reacts with residual lithium (lithium dendrites) leading to considerably higher osmium contents. EELS probing of the bright spots confirms the presence of lithium that coincides with an increased osmium content observed using EDX (Supporting information Fig. S1 and Table S1). The atomic concentration of osmium is 18-fold higher at sites where metallic lithium is present, compared to the rest of the particle where the relatively low osmium concentration is a consequence of the SEI having reacted with OsO_4. These results are in agreement with EDX quantifications performed on stained metallic lithium using SEM (Fig. 2).

Pure metallic lithium foil was further investigated to exploit its favored reaction with osmium tetroxide. Upon staining, lithium metal changed its color from silvery metallic to dark black, became brittle and broke apart whilst handling. This is illustrated in Fig. 2a where the homogeneously covered lithium surface (top left) is fractured exposing a rough sample surface (bottom right). Crystals of osmium reaction products are growing in grass-like shape underneath the removed surface (Fig. 2b and c). The differences in morphology between the surface and the bulk may be explained by a heterogeneous distribution of various lithium species present on the surface of the as received lithium foil or a change of the reaction kinetics due to diffusion limitations for the osmic acid vapor as the thickness of the reaction layer grows. XPS results support the
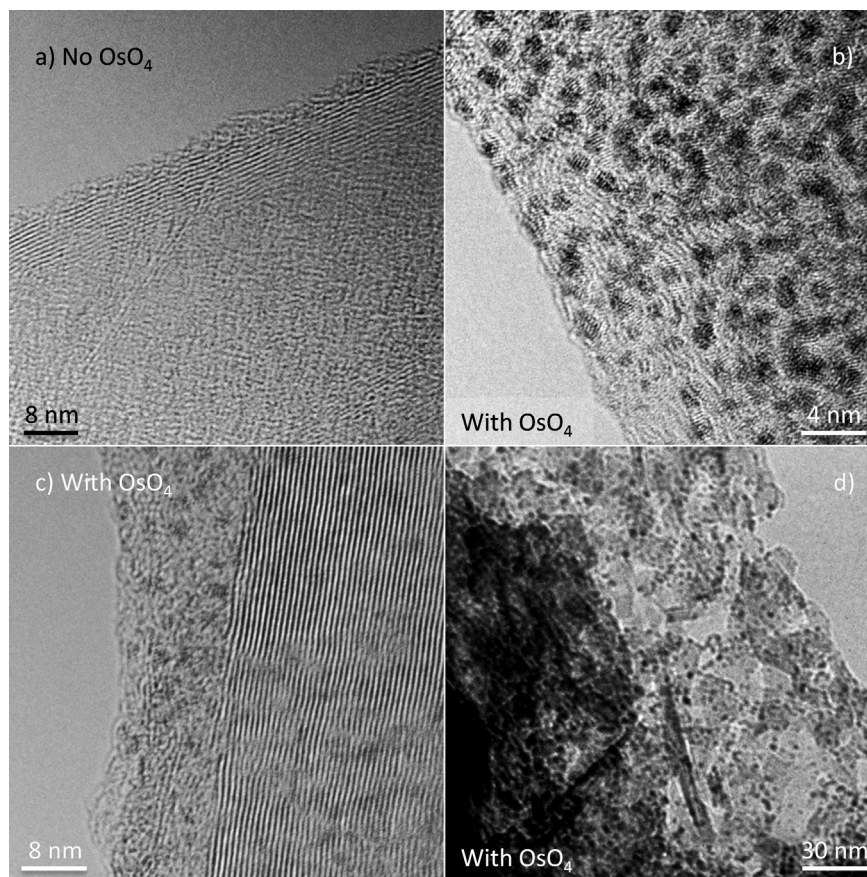
Fig. 1. TEM micrographs of graphite particles with and without osmium tetroxide exposure. (a) HR-TEM of pristine graphite. (b–d), HR-TEM of cycled graphite samples after OsO₄ exposure. The SEI layer of the stained graphite sample is interspersed by nano-sized crystallites of osmium reaction products (b). The sample is covered by the reaction products, yet showing the graphene layers when changing beam focus (c). Preferential reaction sites are visible (d). Osmium tetroxide is reacting selectively, reproducing the heterogeneous structure of the SEI. Translucent phases show almost no reaction. Darker phases exhibit high material contrast due to stronger reaction. The difference might be due to the preferred reaction with double bonds present in the organic components of the SEI.

difference in reactivity towards the surface species and will be discussed later (Fig. 5). The reaction is accompanied by a volume expansion inevitably leading to fracture of the sample. Additionally, the reaction speed at the surface is much higher than in the area below. Whereas the reaction at the surface occurs immediately, it slows down with increasing reaction layer thickness leading to different growth modes. The osmium reaction front grows into the deeper layers of the lithium bulk in a diffusion limited manner creating the unique morphology observed. The sandwich-like structure of the cross-section (Fig. 2d) consists of an about 3 μm layer of dense osmium reaction products on the former lithium surface (to the right of the image), a 10 μm core part interspersed with osmium reaction products as well and a 3 μm thick layer to the left of the image with a columnar growth mode of osmium reaction products. EDX measurements have shown that all three sections had the same osmium content of approximately 30 at.%, hence the composition of the reaction layers is similar and differs in morphology only. An unreacted lithium core was found using XRD on a metallic lithium foil that was exposed to OsO₄ for 24 h (Supporting information Fig. S5). We expect a thorough reaction if the lithium remains exposed for a longer time. However, this will not restrict the application for investigations of lithium dendrites as their dimensions allow for an immediate reaction with osmium tetroxide shown in the following experiments. Yet, a limited reaction speed and diffusion of OsO₄ into the pores of the electrode has to be taken into account in order to choose an appropriate exposure time.

Having sufficiently proven the preferred reaction of osmic acid with metallic lithium it is obvious that the staining technique can be further exploited to detect lithium deposition or residual lithium on electrodes of lithium ion batteries. The elemental contrast aspect of the OsO₄ exposure was studied intensively using scanning electron microscopy (SEM). Experiments were conducted where an etched copper foil, as it is used in current collectors, was electrochemically plated with lithium (charged) that was subsequently removed (stripped) by a reversed current (discharged). According to Faraday's Law the amount of charge is proportional to the amount of lithium deposited/stripped. A coulombic efficiency of 82% indicates that by far not all deposited lithium could be removed from the copper. This can be ascribed to SEI losses occurring as soon as metallic lithium is in contact with the electrolyte and to residual lithium deposits having lost electrical contact ("dead lithium"), therefore remaining on the copper surface [20]. The rinsed copper foil was exposed to osmium and investigated in the SEM. Different dendrite morphologies are found as shown in Fig. 3a–c. The micrographs show intact remaining dendrites (labeled as "Dead Li") that got stained thoroughly with OsO₄ in close vicinity to a bundle of electrochemically stripped dendrites (labeled as "Removed Li") which are visible only by their stained SEI leftovers ("Skins"). The latter ones appear as a hollow shell of electrolyte reduction products having reacted with the OsO₄ vapor still mirroring the initial shape of the dendrites. As shown in the beginning of this section already, the SEI shows a less pronounced reaction with OsO₄ than the metallic lithium, thus exhibiting a much smaller material
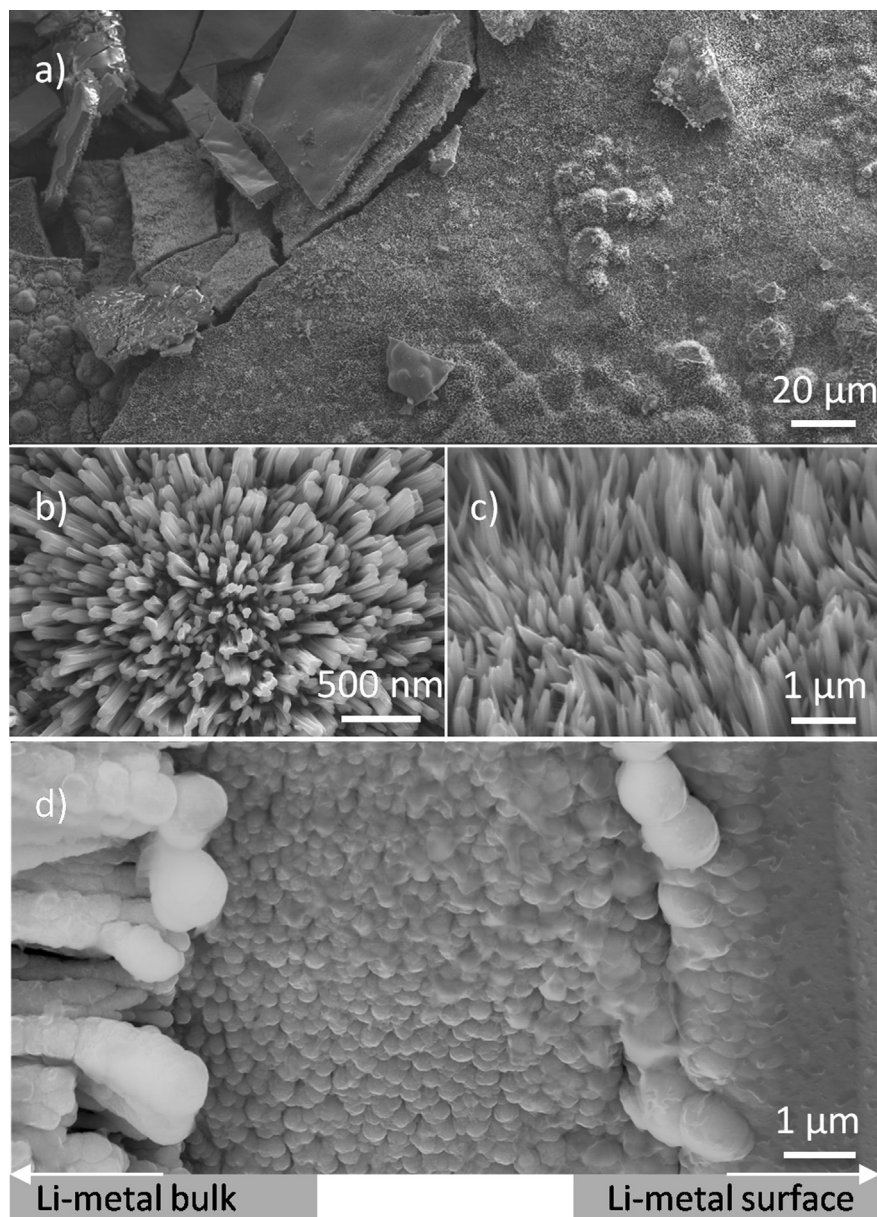
Fig. 2. SEM images of battery grade metallic lithium after 24 h of OsO₄ exposure. (a) Overview showing the cracked Li surface with morphological variations. The former surface (top left of (a) is smooth and homogenously covered whereas the bulk has completely changed its morphology. (b, c) Osmium rich crystallites below the cracked surface in flower like (b) and grass like growth mode (c). (d) Cross sectional view of the stained lithium. Only the uppermost reaction layer of the metallic lithium foil is shown.

contrast in the SEM micrographs of Fig. 3. A direct comparison of a backscattered electron micrograph, solely depicting the differences in elemental weight, and a secondary electron micrograph, preferably describing the morphology, illustrates the highlighting effect very well (Supporting information Fig. S2). Yet another interesting aspect of these results is the little alteration in morphology of the reacted dendrites. There is no evidence of a crystallite-like growth as was the case for metallic lithium foil. The thickness of the dendrites may play a major role. Osmium tetroxide approaches the SEI, reacting with its outer polymeric part, further moving towards the lithium dendrite by gaseous diffusion along the grain boundaries and defects in the SEI. Once it has reached the metallic lithium below, OsO₄ will readily react with lithium dendrites that are much thinner than the bulk lithium foil. A concurrent volume expansion may lead to SEI fracture increasing the pathways for the osmium tetroxide. Hence, the reaction occurs fast and is not limited by

diffusion of a reaction boundary in the same manner as for the bulk metallic lithium. The shape, orientation and size of the dendrites has changed only negligibly whilst staining. It seems as if they have grown randomly and not necessarily in the direction of the counter electrode. Some are being deflected quite often, also appearing in different thicknesses. This non-uniform growth can easily lead to mechanical interaction among dendrites causing the loss of electrical contact. No greater beam damage was observed where osmium staining had taken place. Even subtle structures like the "SEI-skins" of stripped dendrites (Fig. 3) remained stable in the electron beam. Thus it appears that osmium reaction products provide a stabilization of the SEI components making them more accessible to electron microscopy investigations.

For a quantitative measure of the lithium dendrites, electrochemical results are compared to energy dispersive x-ray spectroscopy (EDX) data in dedicated plating experiments. When
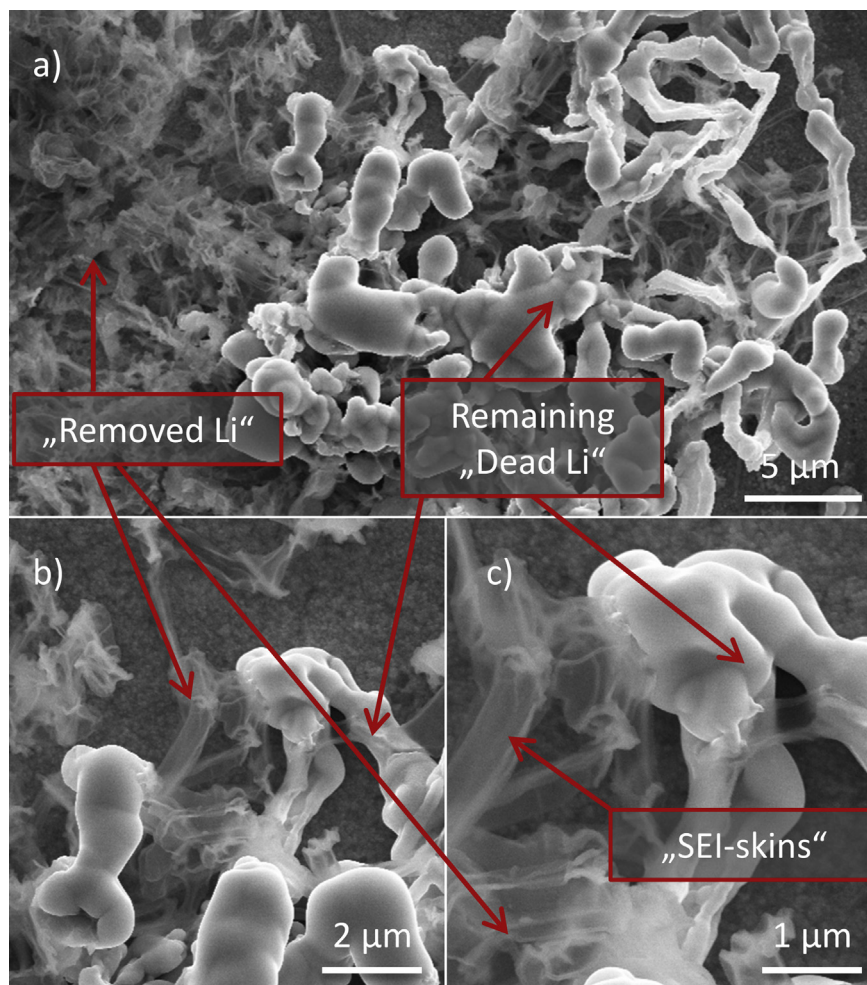
Fig. 3. Appearance of lithium dendrites on a copper electrode after OsO₄ exposure. The metallic lithium was deposited electrochemically in constant current mode and was stripped off electrochemically thereafter by applying a constant current of the same rate in the opposite direction. The coulombic efficiency of the charge/discharge cycle was determined to be 82%. (a–c) Arrows indicate i) the remaining "dead lithium" and ii) the leftovers of electrochemically removed lithium. Latter ones (its electrolyte reaction (SEI) layer has reacted with the OsO₄) can be clearly distinguished from the very prominent intact lithium dendrites that have readily reacted with OsO₄. The shape of both remains almost untouched by the staining reaction allowing conclusions on growth mode and extend.

electrochemically depositing a certain amount of lithium, the amount of osmium detected by EDX should be proportional to the amount of lithium that can be calculated from the charge consumed using Faraday's law. For least influence of the supporting matrix, pure copper discs were used as electrodes. The electrochemical and EDX results of such an experiment with different amounts of lithium deposited are shown in Table 1. Dividing the amount of osmium on the sample by the mass of lithium equivalent to the charge transferred electrochemically, shows that the amount of osmium detected by EDX scales linearly with the amount of lithium deposited. An uncertainty in the results arises from the part of lithium reacting with the electrolyte, therefore causing a different reaction with OsO₄. The deviation may only cause errors in case of very small amounts of lithium deposited or with very fine plating, where the ratio of metallic lithium to dendrite surface is relatively low. The EDX results have shown that the OsO₄ staining technique allows to determine the relative amount of lithium deposited on plated electrode surfaces.

The unique visibility of the dendrites can be also used to further study lithium distribution, areas of preferred growth, and area specific quantification of lithium deposition, especially on graphite anodes, by far exceeding the capabilities of electron microscope imaging on unstained samples. Fig. 4 gives an overview

of means to verify dendrites with (Fig. 4e–h) and without (Fig. 4a–d) osmium tetroxide staining. Excitation voltage, aperture and working distance of the electron microscope is adjusted from Fig. 4a to b and Fig. 4c to d for an optimized visibility of lithium dendrites with respect to the graphite base material. A highlighting effect is successfully achieved improving with increasing magnification, however, being consumed by edge effects of the graphite particles at lower magnification quickly (Fig. 4d). Fig. 4e–h shows a combination of SE imaging and EDX mapping. Very good singularization of the lithium deposits is achieved in Fig. 4g supported by the EDX mapping in Fig. 4h. Stained lithium dendrites can be well distinguished from graphite even at lower magnifications, enabling an easy detection at low magnifications also. Thus, distribution of dead-lithium across the surface of graphite electrodes can be studied conveniently. Another difficulty of detection usually arises at sites where lithium was almost fully removed electrochemically (Fig. 4e and f). Only little information can be obtained from the SE-images despite the use of osmic acid. However, the combination with EDX mapping accentuates even the locations where lithium deposits had formed before through the stained SEI residues. This allows an unprecedented way to localize sites of lithium growth even though the lithium is not present anymore.

Without OsO₄ staining   **With OsO₄ staining**
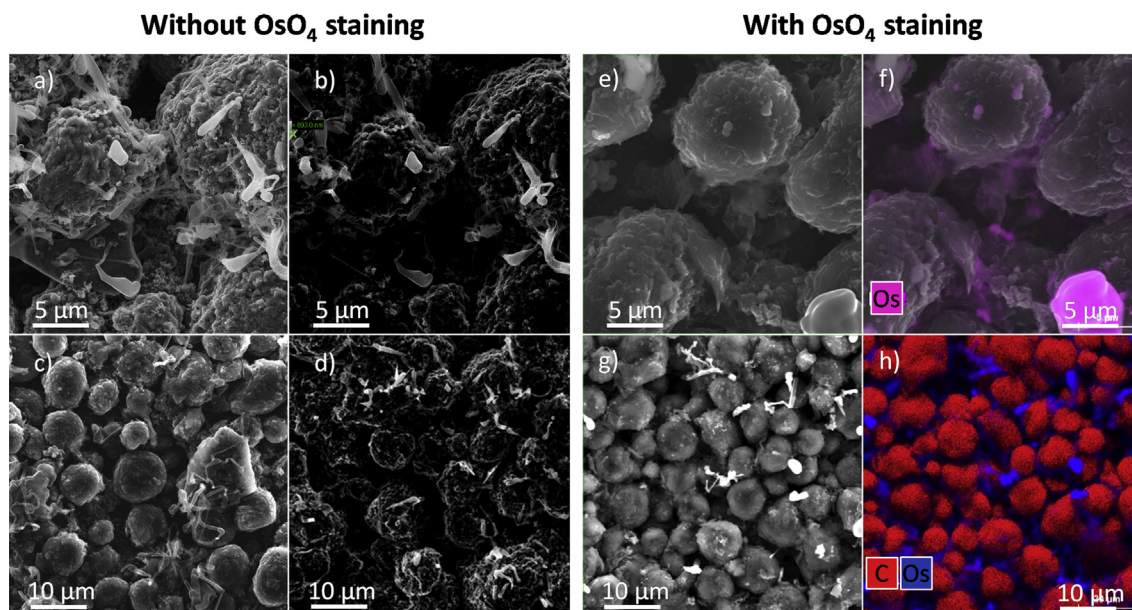
Fig. 4. Visibility of lithium deposition on graphite electrodes with and without OsO₄ treatment using a combination of SE imaging and EDX mapping. (a–d) SE images of unstained electrodes. Aperture, working distance, excitation voltage and exposure was optimized from (a) to (b) and (c) to (d) in order to accentuate the lithium deposits with respect to the graphite. (e–h) SE images of OsO₄ treated electrodes. Whereas an area with removed dendrites (e) shows almost no material contrast despite OsO₄ staining, the corresponding EDX mapping (f) overcomes invisibility of empty SEI skins that testify the presence of lithium dendrites that have been removed electrochemically. Lower magnification image of the electrode exhibits good material contrast using secondary electron imaging (g). The element map (h) for carbon (red) and Os (blue) supports the highlighting effect of the osmium reaction. All electrodes have been subject to electrochemically forced lithium deposition (overcharge) and removal (full discharge) prior to the staining treatment. (For interpretation of the references to color in this figure legend, the reader is referred to the web version of this article.)

In order to obtain less localized information on the lithium distribution, lower magnifications have to be used. A comparable adjustment of the electron microscope does not exhibit the highlighting effect that can be achieved using high magnifications as described above. Yet, the enhanced material contrast of osmium reaction products tremendously extends the visibility (Supporting information Fig. S4). Therefore first experiments were realized exploiting the emphasis of osmium in the SEM in backscattered mode. The very bright osmium reaction sites stand out from the matrix of lighter elements. Adjusting contrast and brightness, this effect can be used to create threshold pictures (Supporting information Fig. S4) that can be quantitatively analyzed for their area fractions. Systematic studies of lithium quantification in combination with the threshold method are underway.

Despite the many advantages, side reactions with intercalated lithium are likely to occur due to the highly oxidative behavior of the Os^{8+}. To avoid misinterpretation of the results, care has to be taken on a thoroughly discharge of the graphite, as was done for all of our samples prior to exposure. Yet, we cannot exclude, that the lithium found in the specific sample of TEM Fig. S1 represents a feature of chemical deintercalation of the graphite. Albeit this basically undesired reaction, we are currently investigating the advantages thereof. When lithium is removed from the graphite, this process is restricted to preferential sites of the graphite, e.g. the prismatic planes. Thus, lithium can only exit through defined diffusion paths and flaws which could be highlighted by the staining technique.

3.2. Reaction mechanism

Osmium tetroxide is known to react with double bonds and as a strong Lewis acid may also attack carboxyl groups, alcohols, amines, esters and ethers. It has also been shown to stain grain boundary regions between amorphous and crystalline parts of
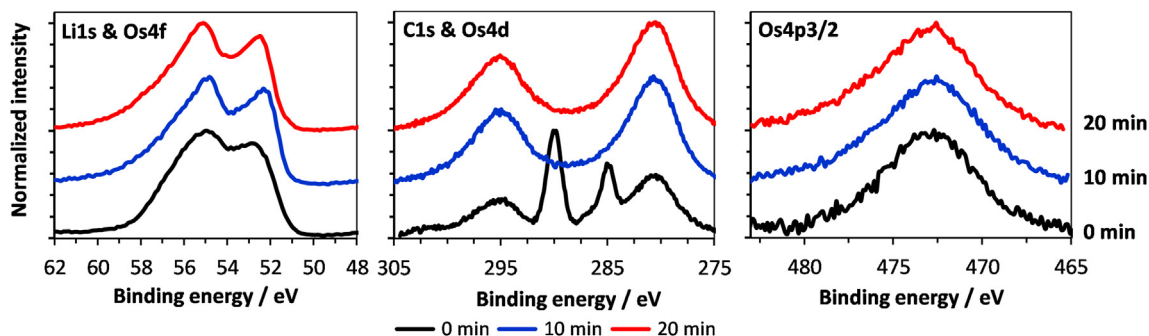
Fig. 5. XPS spectra of metallic lithium after OsO₄ exposure. Sputtering reveals differences in composition. The XPS signals of a stained lithium metal sample change during sputtering showing differences between reaction products on the surface and in the bulk. Each of the two argon sputtering cycles shown removed about 50 nm of material from the surface. The composition remains the same after about 50 nm. An overlap of Os 4f signals with Li 1s can be seen. An even stronger overlap of energies is present for the Os 4d and C1s energies.

Table 1
EDX quantification of lithium deposited on copper foil exposed to OsO_4. Values for C, Cu, F, O and P (electrolyte components) are not shown here but were considered for quantification.

Li deposited (mAh)	Equiv. Amount of lithium (µg)	Amount of Os detected		Os : Li ratio (wt.% µg^{-1})	Os : Li ratio (at.% µg^{-1})
		Os (wt.%)	Os (at.%)		
0.01	2.6	1.9	0.5	0.73	0.19
0.30	77.7	57	13.7	0.73	0.18

polyethylene or polypropylene polymers ethers [48]. Thus, a reaction with reduced organic parts of the SEI containing double bonds, but also polycarbonates or lithium alkyl carbonates, which have been shown to compose the organic part of the SEI layer [28], is very likely. Although the exact staining reactions still need to be clarified it is clearly evidenced by the TEM and SEM results in Figs. 1 and 3 that a reaction with parts of the SEI layer occurs. However, due to the highly oxidative nature of OsO_4 there is also a strong driving force of OsO_4 to react with metallic lithium or lithiated graphite. As the osmium reaction has so far not been investigated using materials for energy storage, elucidating the reaction mechanism will help interpreting the spectroscopic and morphological results. Metallic lithium turns from silver color to shiny black on the surface after osmium exposure as does lithium that was deposited on top of a graphite electrode. For the highly reactive lithium it would be straight forward to expect the following reaction path forming the stable Os (IV) oxide and lithium oxide:

$$4\,Li + OsO_4 \rightarrow 2Li_2O + OsO_2 \tag{1}$$

The black color though, does reflect neither the lithium oxide nor the osmium (IV) oxide. This suggests that different reaction products have formed. XRD measurement of the lithium bulk that has not reacted thoroughly, as well as explicit measurement of the black reaction layer present on metallic lithium is displayed in Supporting information Fig. S5. The high background at lower Bragg angles originates from the Kapton foil used to fix the sample. No binary osmium compounds can be fitted using the Inorganic Crystal Structure Database, neither the expected lithium oxide nor other lithium compounds such as LiOH and Li_2CO_3. Therefore we expect the osmium tetroxide to react with lithium by forming a ternary $Li_xOs_yO_z$ compound. Known ternary osmium compounds containing lithium are reported to be Li_5OsO_6 [49], Li_6OsO_6 [50], Li_7OsO_6 [51]. However, none of the reported structures fits the measured patterns well. A minor contribution of the Li_7OsO_6 phase could be found but does not represent the main phase. With respect to the oxidation state of this structure, a low oxidation state of osmium (here +V) appears more likely to have formed than the high oxidation states in Li_5OsO_6 and Li_6OsO_6 being +VII and +VI, respectively. Hence, a more detailed structural investigation of lithium–osmium compounds would be necessary to precisely identify the reaction products formed but is beyond the scope of this manuscript. The broadness of the peaks yet accounts for the nano-size of the particles already observed using TEM. Apparently a much more complex reaction than Equation (1) occurs on the surface. The low temperature and the high speed at which the reaction takes place leads to a reaction product with high defect density absorbing most parts of the visible light, therefore appearing black. XPS measurements of a pristine graphite after osmium tetroxide exposure (not presented in this paper) show that there is no remarkable staining effect on the pure carbon active material. Hence, experimental results should not be corrupted by a hidden graphite reaction.

Battery grade lithium metal, exposed to OsO_4, was probed for the chemical bonding of the osmium species formed. Additional depth profiling of the stained lithium foil shows a prominent change of the spectra, indicating differences in the reaction of surface and bulk (Fig. 5).

In the C 1s spectra the polyolefin contamination and carbonate peak of the stained lithium surface (pronounced peaks at ~284.8 eV and ~290 eV) with two satellite-like peaks at 295 eV and 280 eV can be seen. As the lithium surface is almost always covered by trace contaminants, the carbonate peak is a regular feature of the lithium XPS-spectrum. The two satellite peaks can be attributed to the Os 4d binding energies that overlap with the C 1s energy levels. Upon sputtering, the C—O and C]O peaks have vanished revealing the Os 4d peaks. Applying a second sputtering cycle, the energies and intensities remain the same in comparison to the first one. Having removed about 100 nm it becomes obvious that the osmium tetroxide does not only react at the surface of metallic lithium as was already evident from the SEM measurements of the metallic lithium foil. The shape of the osmium satellites does not change upon surface removal, thus the reaction products formed should be of the same nature.

In the Li 1s spectrum a broad peak between 54 eV and 56 eV represents the main surface contaminations of the lithium metal, Li_2O and Li_2CO_3. The other peak is correlated to the Os 4f signal at 52 eV (OsO_2). Further Os 4f contribution can be found at energies >57 eV, however, metallic osmium (50 eV) is not present. The Li 1s binding energies do not change significantly upon sputtering showing that the osmium reaction products are the same but differ with respect to their relative amounts. Yet a small deviation in the high energy shoulder is observed upon sputtering. It can be assumed that this refers to different osmium reaction products in comparison to the species present on the surface. However, this change is also likely to be induced by the reductive argon ions and is therefore a consequence of the sputtering process but not an intrinsic sample property.

The main peak energy in the Os 4p3/2 spectrum is located at 472.7 eV. Metallic osmium corresponds to energies of 470.7 eV and OsO_2 to 472.9 eV [52]. This indicates that osmium is in a similar chemical environment as in OsO_2 and has an oxidation state of +IV. However, the peak width indicates that there may be other osmium compounds with higher and lower binding energies as well. With respect to the XRD and XPS data, we propose a lithium osmate $Li_xOs_yO_z$ which contains osmium most likely in an oxidation state of +IV. The broad peaks indicate the existence of more complex Li—O—Os compounds with various bonding energies.

The osmium energies overlap with energies from Li 1s and C 1s. The Os 4d energies are located at about 297 eV (4d3/2) and 282 eV (4d5/2) and thus in close proximity to the carbonate and contamination peak of the C—O bonding energies. A similar effect is even more severe for the lithium specific energies. Os 4f signals (52 eV–62 eV) overlap with the Li 1s spectrum as can be seen in Li 1s energies of Fig. 5. Hence, lithium is being over-determined. The ratio of Li to Os content in the sample is difficult to obtain as the osmium signals suppress the lithium signal. A correction of the sensitivity factor is essential. Seemingly, high osmium intensities in the XPS spectra do not automatically correspond to high osmium contents in the sample. The atomic concentration of osmium rises from
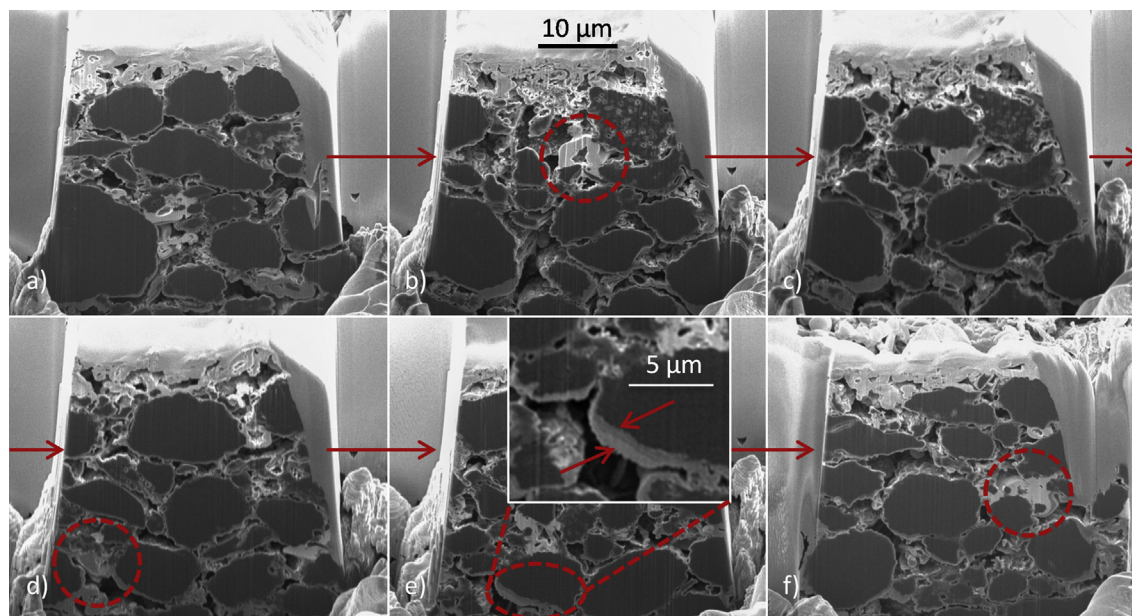
Fig. 6. SEM images of the cross section of a graphite electrode at different stages during the slice and view procedure. (a—f) The highlighted areas show characteristic features of the staining procedure. The top of the electrode is covered with lithium dendrites exhibiting a high material contrast due to their strong reaction with OsO$_4$ (b). Lithium deposits can also be found within the electrode (circles in (b) and (f)) partly clogging pore space. Differences in the SEI layer surrounding the graphite particles are visible (circles in (d) and (e)) revealing variations in thickness. These differences are especially obvious in (e) where a multilayer structure can be deduced from varying material contrast. A fly-through movie of all 250 slices can be found in the supporting information.

0.8 at.% before to 3 at.% after sputtering which is not in agreement with the TEM-EDX and SEM-EDX results. As the penetration depth of XPS is less than 50 Å, and 100 nm of the lithium surface layer were removed only, we can conclude that the argon sputtering has not exposed the main reaction phase.

3.3. Slice and view

Cycled and purposely overcharged graphite composite electrodes were fully discharged and subsequently exposed to OsO$_4$. After 12 h exposure the samples were cut on a dual beam device for cross-sectional investigations using a slice-and-view technique as explained in the experimental section. In total, 250 slices were removed in a step by step procedure with a step size of 105 nm. The series of images was used to create a fly-through movie that can be found in the Supporting information.

Analyzing the cross-sectional images, heterogeneities in contrast and thickness of the layers surrounding the graphite particles are visible (Fig. 6). The dark-grey areas represent the graphite. The surrounding SEI layer commonly appears brighter due to the osmium staining that leads to a stronger inelastic interaction of electrons with the material. A third, very bright level can be attributed to osmium-rich lithium residues.

As highlighted in Fig. 6d and e, the graphite particles are covered by a layer that is consistently thicker towards the bottom part of the electrode. In some places (Fig. 6b and d) this layer is almost clogging the pores by its dimensions, remaining less than 2 μm in thickness, though. Looking more in detail (bottom of Fig. 6e), some of the graphite particles are covered by two layers of different contrast. The brighter one seems to have grown on top of the one closer to the graphite. As there is a relatively distinct interface between both layers the difference in contrast is neither an artifact nor does it originate from lithium deposits breaking through the SEI. The split layer could rather be due to a change in composition of the multilayer SEI whilst cycling [53,54], e.g. a thicker organic outer layer or less conductive reaction products appearing brighter in the SEM.

Additionally, the lithium residues react more vigorously with osmium tetroxide. These areas of very high osmium content appear even brighter than the stained graphite cocoons. According to our earlier investigations they can be attributed to metallic lithium, i.e. lithium dendrites. Most of which can be found on the electrodes' surface where worm-like structures can be distinguished from the bulk platinum pad above. Surprisingly, these are not limited to the surface of the electrode. Areas of equivalent contrast are nestled to the porous particle framework. They are several micrometers in size and separate themselves clearly from the surroundings in terms of contrast. A pseudo color image (graphical abstract) highlights the different material contrasts, revealing graphite, SEI and lithium dendrites. One might have expected lithium to also grow within the graphite composite electrode. The extent of the lithium dendrites however is unexpected. To the best of our knowledge no investigations concerning lithium dendrite distribution across the electrode have been published so far. Due to the close vicinity of the potential of fully charged graphite to that of metallic lithium, the electrode potential is likely to drop below the actual lithium deposition potential. The complex current distribution within the porous electrode leads to local potential differences that can hardly be estimated [25]. Drops in potential down to values below lithium deposition are inevitable on the particle level although the overall electrode potential recorded may still be above 0 V against Li$^+$/Li. Hence the complex morphology of the porous electrode represents a fertile soil for lithium deposition making it almost impossible to control lithium plating throughout the electrode. The volatile osmium tetroxide vapor represents a valuable means to analyze composite electrode cross sections for their lithium dendrite distribution and the evolution of the SEI layer.

4. Conclusion

Osmium tetroxide staining was successfully applied to graphite anodes and metallic lithium tremendously improving contrast in electron microscopy. Similar to the fixation of tissue in biology and

medicine we were able to minimize the damage inflicted on the sample by the electron beam in the SEM or TEM. The reaction of osmium tetroxide with the SEI allows for an improved visibility in TEM making it clearly distinguishable from the graphite it surrounds. This opens up new possibilities to investigate the evolution of the SEI over the life time of battery anodes gaining a better understanding of the electrode/electrolyte interface. Our studies have shown that metallic lithium intensely reacts with osmium tetroxide. Hence, we were able to highlight lithium dendrites on the surface and within the cross section of graphite electrodes in the electron microscope for the first time. Offering an increased material contrast, the osmium reaction products allowed to substantially improve detection and quantification of lithium deposits. The material contrast as well as the small change in dendrite morphology invoked by the reaction can be further utilized to ease the investigation of dead lithium on graphite electrodes. In combination with EDX, the technique offers the quantification and mapping of distribution of "dead lithium" on graphite electrodes. EDX can be furthermore used localize sites of lithium deposition through their stained SEI shells even though the lithium has been removed electrochemically already.

An additional stability of the sample under ambient air was achieved. Stained samples did not show any reactions with air moisture for an extended amount of time compared to unstained ones (Supporting information Fig. S3). We further believe that this technique can be well applied to other anode materials, although the OsO_4 staining appeared most efficient in the case of enhancing poor elemental contrast in graphite electrodes. Yet, the exact reaction mechanism remains ambiguous and will be part of future investigations. The formation of ternary $Li_xOs_yO_z$ compounds was proposed based on XPS and XRD results. Owing to the versatility of the technique, further efforts will help to fully exploit its potential for lithium battery research.

Acknowledgments

Appendix A. Supplementary data

Supplementary data related to this article can be found at http://dx.doi.org/10.1016/j.jpowsour.2014.04.134.

References

[1] L. Gireaud, S. Grugeon, S. Laruelle, B. Yrieix, J.-M. Tarascon, Electrochem. Commun. 8 (2006) 1639.
[2] O. Crowther, A.C. West, J. Electrochem. Soc. 155 (2008) A806.
[3] M.C. Smart, B.V. Ratnakumar, J. Electrochem. Soc. 158 (2011) A379.
[4] C. Brissot, M. Rosso, J.N. Chazalviel, S. Lascaud, J. Power Sources 81 (1999) 925.
[5] F. Ding, W. Xu, X. Chen, J. Zhang, M.H. Engelhard, Y. Zhang, B.R. Johnson, J.V. Crum, T.A. Blake, X. Liu, J.-G. Zhang, J. Electrochem. Soc. 160 (2013) A1894.
[6] M.S. Park, S.B. Ma, D.J. Lee, D. Im, S.-G. Doo, O. Yamamoto, Sci. Rep. 4 (2014) 3815.
[7] L. Suo, Y.-S. Hu, H. Li, M. Armand, L. Chen, Nat. Commun. 4 (2013) 1481.
[8] N. Gunawardhana, N. Dimov, M. Sasidharan, G.-J. Park, H. Nakamura, M. Yoshio, Electrochem. Commun. 13 (2011) 1116.
[9] H. Honbo, K. Takei, Y. Ishii, T. Nishida, J. Power Sources 189 (2009) 337.
[10] G. Park, N. Gunawardhana, H. Nakamura, Y. Lee, M. Yoshio, J. Power Sources 196 (2011) 9820.
[11] G. Park, N. Gunawardhana, H. Nakamura, Y.-S. Lee, M. Yoshio, J. Power Sources 199 (February 2012) 293—299.
[12] J.K. Stark, Y. Ding, P.A. Kohl, J. Electrochem. Soc. 158 (2011) A1100.
[13] J.K. Stark, Y. Ding, P.A. Kohl, J. Electrochem. Soc. 160 (2013) D337.
[14] K.P. Doyle, C.M. Lang, K. Kim, P.A. Kohl, J. Electrochem. Soc. 153 (2006) A1353.
[15] F. Ding, W. Xu, G.L. Graff, J. Zhang, M.L. Sushko, X. Chen, Y. Shao, M.H. Engelhard, Z. Nie, J. Xiao, X. Liu, P. V Sushko, J. Liu, J.-G. Zhang, J. Am. Chem. Soc. 135 (2013) 4450.
[16] S.J. Harris, A. Timmons, D.R. Baker, C. Monroe, Chem. Phys. Lett. 485 (2010) 265.
[17] D. Aurbach, Y. Cohen, J. Electrochem. Soc. 143 (1996).
[18] S. Chandrashekar, N.M. Trease, H.J. Chang, L.-S. Du, C.P. Grey, A. Jerschow, Nat. Mater. 11 (2012) 311.
[19] I.W. Seong, C.H. Hong, B.K. Kim, W.Y. Yoon, J. Power Sources 178 (2008) 769.
[20] F. Sagane, R. Shimokawa, H. Sano, H. Sakaebe, Y. Iriyama, J. Power Sources 225 (2013) 245.
[21] K.J. Harry, D.T. Hallinan, D.Y. Parkinson, A.A. Macdowell, N.P. Balsara, Nat. Mater. 13 (2014) 69.
[22] R. Bhattacharyya, B. Key, H. Chen, A.S. Best, A.F. Hollenkamp, C.P. Grey, Nat. Mater. 9 (2010) 504.
[23] F. Orsini, A. Du Pasquier, B. Beaudoin, J.M. Tarascon, J. Power Sources 76 (1998) 19.
[24] M. Tang, P. Albertus, J. Newman, J. Electrochem. Soc. 156 (2009) A390.
[25] D. Kehrwald, P.R. Shearing, N.P. Brandon, P.K. Sinha, S.J. Harris, J. Electrochem. Soc. 158 (2011) A1393.
[26] E. Peled, J. Electrochem. Soc. 126 (1979) 2047.
[27] J. Vetter, P. Novák, M.R. Wagner, C. Veit, K.-C. Möller, J.O. Besenhard, M. Winter, M. Wohlfahrt-Mehrens, C. Vogler, A. Hammouche, J. Power Sources 147 (2005) 269.
[28] P. Verma, P. Maire, P. Novák, Electrochim. Acta 55 (2010) 6332.
[29] D. Aurbach, E. Zinigrad, Y. Cohen, H. Teller, Solid State Ionics 148 (2002) 405.
[30] J.T. Lee, N. Nitta, J. Benson, A. Magasinski, T.F. Fuller, G. Yushin, Carbon 52 (2013) 388.
[31] F. Kong, R. Kostecki, G. Nadeau, X. Song, K. Zaghib, K. Kinoshita, F. McLarnon, J. Power Sources 97-98 (2001) 58.
[32] G.V. Zhuang, K. Xu, T.R. Jow, P.N. Ross, Electrochem. Solid-State Lett. 7 (2004) A224.
[33] A.M. Andersson, K. Edström, J. Electrochem. Soc. 148 (2001) A1100.
[34] K. Edström, M. Herstedt, D.P. Abraham, J. Power Sources 153 (2006) 380.
[35] S. Bhattacharya, A.T. Alpas, Carbon 50 (2012) 5359.
[36] S. Chattopadhyay, A.L. Lipson, H.J. Karmel, J.D. Emery, T.T. Fister, P.A. Fenter, M.C. Hersam, M.J. Bedzyk, Chem. Mater. 24 (2012) 3038.
[37] M. Nie, D. Chalasani, D.P. Abraham, Y. Chen, A. Bose, B.L. Lucht, J. Phys. Chem. C 117 (2013) 1257.
[38] C.K. Chan, R. Ruffo, S.S. Hong, Y. Cui, J. Power Sources 189 (2009) 1132.
[39] K. Kato, J. Polym. Sci. Part B Polym. Lett. 14 (1966) 219.
[40] C. Scala, G. Cenacchi, R.P. Apkarian, P. Preda, G. Pasquinelli, J. Electron Microsc. (Tokyo) 39 (1990) 508.
[41] T. Voigt, W. Dauber, I. Bensemann-Ryvkin, X. Härtel, Microsc. Res. Tech. 58 (2002) 121.
[42] F. Di Scipio, S. Raimondo, P. Tos, S. Geuna, Microsc. Res. Tech. 71 (2008) 497.
[43] L.H. Sperling, in: D. Klempner, K.H. Sperling, L.A. Utracki (Eds.), Interpenetr. Polym. Networks, 239th ed., American Chemical Society, 1994, pp. 3—38.
[44] F.J. Baltá Calleja, L. Giri, G.H. Michler, I. Naumann, Polym. (Guildf.) 38 (1997) 5769.
[45] H.J. Sue, E.I. Garcia-Meitin, B.L. Burton, C.C. Garrison, J. Polym. Sci. Part B Polym. Phys. 29 (1991) 1623.
[46] M.A. Parker, D. Vesely, Microsc. Res. Tech. 24 (1993) 333.
[47] E. Peled, J. Electrochem. Soc. 144 (1997) L208.
[48] M. Dekker, in: G.O. Shonaike, G.P. Simon (Eds.), Polym. Blends Alloy., CRC Press, 1999, p. 768.
[49] T. Betz, R. Hoppe, Z. Anorg. Allg. Chem. 524 (1985) 17.
[50] J. Hauck, Z. Naturforsch. 24b (1969) 1067.
[51] C. Mühle, A. Karpov, A. Verhoeven, M. Jansen, Z. Anorg. Allg. Chem. 631 (2005) 2321.
[52] J. Moulder, J. Chastain, R. King, Handbook of X-Ray Photoelectron Spectroscopy: A Reference Book of Standard Spectra for Identification and Interpretation of XPS Data, Illustrate, Physical Electronics, Eden Prairie, 1995.
[53] J. Thevenin, R. Muller, J. Electrochem. Soc. 134 (1987) 273.
[54] H. Bryngelsson, M. Stjerndahl, T. Gustafsson, K. Edström, J. Power Sources 174 (2007) 970.